Design and performance of an integrated fluorescence, polarized fluorescence, and Brewster angle microscope/Langmuir trough assembly for the study of lung surfactant monolayers

Michael M. Lipp, Ka Yee C. Lee, and Joseph A. Zasadzinski
Department of Chemical Engineering, University of California, Santa Barbara, California 93106

Alan J. Waring
Department of Pediatrics, King/Drew University Medical Center and Perinatal Laboratories, Harbor-UCLA School of Medicine, Los Angeles, California 90059

(Received 18 September 1996; accepted for publication 17 February 1997)

We describe an integrated fluorescence, polarized fluorescence, and Brewster angle microscope/Langmuir trough assembly. This apparatus was specifically designed for the study of lung surfactant (LS) monolayers, and is well suited for the study of other lipid/protein monolayer systems. The apparatus can be operated simultaneously in both the fluorescence and Brewster angle modes under a wide range of conditions, including physiological subphases and temperatures. The combination of information obtained from these microscopy techniques facilitates the identification of the composition of coexisting phases, allows us to systematically study the effects of specific proteins on lipid monolayers, and eliminates possible artifacts inherent to fluorescence. To demonstrate this system we present images of mixed monolayers of the anionic and unsaturated lipid components of LS and show that synergistic interactions between certain LS proteins and these lipids hold the key to the proper functioning of LS monolayers. © *1997 American Institute of Physics.* [S0034-6748(97)00606-0]

I. INTRODUCTION

The study of mixed lipid and protein monolayers can yield information on basic biological phenomena such as membrane function and enzymatic processes at interfaces, as well as provide a foundation for biosensor design and two-dimensional protein crystallization.[1–3] The lipid and protein monolayer at an air/water interface is also an ideal model for the study of lung surfactant (LS), which forms monolayers at the air/water interface in the alveoli of air breathing animals, including humans. Direct monolayer imaging techniques such as fluorescence and Brewster angle microscopies have allowed the visualization of phase transitions occurring in monolayers.[3–9] Fluorescence microscopy (FM) has been used to determine domain sizes and shapes during these transitions, and also to directly monitor such processes as proteolytic enzyme activity on phospholipid monolayers.[10,11] Both polarized fluorescence (PFM) and Brewster angle (BAM) microscopies have been put to similar use, and can provide additional information on lipid ordering such as hydrocarbon chain tilt in condensed phase domains.[12,13] However, little FM or BAM has been done on LS, especially monolayers containing lung surfactant-specific proteins.[14–16] We have designed a combined FM, PFM, and BAM microscopy system that is well suited for the study of LS monolayers as well as other lipid/protein systems. The combined assembly provides an ideal system for the elucidation of the mechanism of action of both natural and synthetic LS systems.

Natural LS consists of a mixture of lipids and proteins, the combination of which provides for rapid adsorption to the alveolar air/water interface and formation of a monolayer that can achieve low surface tensions. The major lipid found in natural LS is dipalmitoylphosphatidylcholine (DPPC), which plays a primary role in lowering the monolayer surface tension.[17] However, LS also contains significant amounts of anionic and unsaturated lipids as well as two surface-active proteins, SP-B and SP-C. The complete roles of these components are not yet understood,[18,19] but they are known to be essential for the proper functioning of LS *in vivo* and in replacement surfactants for the treatment of respiratory distress syndrome. SP-B in particular has been shown to greatly increase the activity of LS lipids both *in vitro* and *in vivo*; it has also been shown that simple peptide sequences based on the amino terminus of SP-B possess the full activity of the native protein.[20–24] It has been proposed that the unsaturated and anionic lipids together with the protein components act to enhance adsorption rates of LS by fluidizing the DPPC-rich mixture, however, their presence and fate in the resulting monolayer is unknown at present. The anionic and fluidizing lipids in LS alone form monolayers that collapse before they can achieve low surface tensions. This has called into question their ability to remain in LS monolayers containing DPPC up to collapse, and has led to the development of a ''squeeze-out'' hypothesis which states that these components are selectively removed from LS monolayers to leave them enriched in DPPC.[25] There is evidence that some unsaturated lipid components of LS are squeezed out of binary monolayers containing DPPC or dipalmitoylphosphatidylglycerol (DPPG) once certain surface tensions are reached.[26,27] However, such binary lipid monolayers do not adequately represent the functioning LS monolayer; synergistic interactions between LS lipids and proteins alter this process and may remove the driving force for squeeze-out of the fluidizing components.

Our combined microscopy system is well suited to answer questions such as these, as well as for studying the

 0034-6748/97/68(6)/2574/9/$10.00

general phase behavior and collapse mechanics of lipid and protein monolayers. FM is an ideal technique to study the influence of protein on monolayers of lipids found in LS. Labeling LS proteins such as SP-B and SP-C with fluorescent tags allows us to confirm their presence in monolayers up to the point of collapse, as well as quantify their effects on the phase behavior of the LS lipids. These dual-probe studies, in which the fluorescence from both lipid probes and labeled proteins are monitored simultaneously, allows us to determine the partitioning of the proteins between phases. FM also permits us to pinpoint the location and structure of the three-dimensional collapsed phases in these systems, and to track the removal of lipid into the subphase prior to collapse. PFM shows the effects of the protein on the ordering of the lipid-rich condensed phases (i.e., the presence or absence of tilt contrast) and on the structure of the collapsed phase. BAM provides images of these monolayers by utilizing the fact that at the Brewster angle for the air/water interface, *p*-polarized light is weakly reflected by monolayers. The intensity of the reflected light being a function of the local state of the monolayer, variations in the refractive index of the monolayer will result in a contrast. Thus, BAM permits us to study these monolayers without requiring the presence of fluorescent tags, confirming that the fluorescent probe molecules at low mole percentages do not influence the phase behavior seen via FM and PFM, and providing information on local tilt or other anisotropic orientational effects. The complementary information obtained by FM, PFM, and BAM can also facilitate the identification of the compositions of various coexisting phases when studying monolayers containing multiple components, which will be crucial in attempts to systematically study multicomponent model LS monolayers.

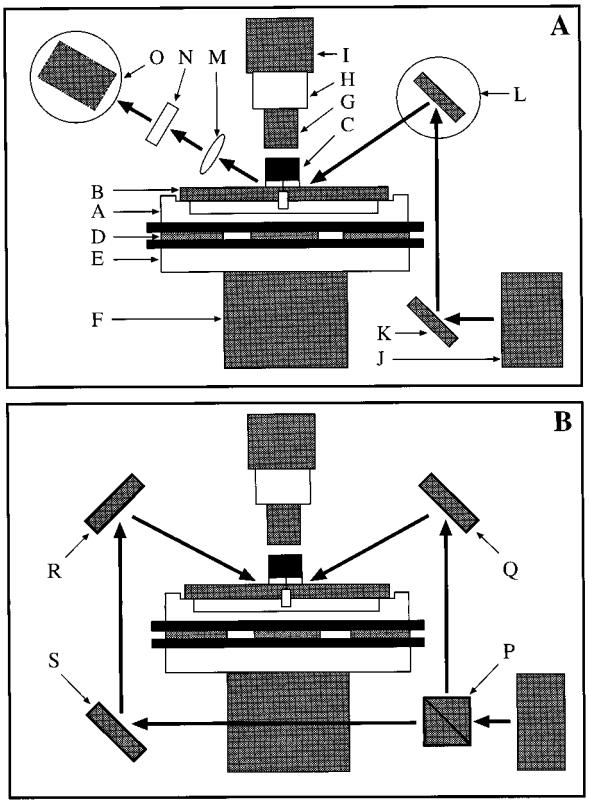

FIG. 1. A schematic of the FM/PFM/BAM assembly. (**A**) Configuration for dual FM/BAM operation. The labeled parts are: (A) Langmuir trough, (B) barrier, (C) surface pressure sensor, (D) thermoelectric elements, (E) water bath, (F) motorized *xyz* translation stage, (G) microscope objective, (H) mercury lamp/fluorescence filter cube assembly, (I) SIT camera, (J) laser, (K) mirror, (L) rotatable mirror, (M) lens, (N) polarizer cube (analyzer), (O) CCD camera (mounted on a rotatable stage). (**B**) Configuration for PFM operation. The parts specific to the PFM are (including the laser): (P) beamsplitter cube, (Q, R, S) mirrors. The bold arrows in both drawings denote the light path of the laser beam in the BAM and PFM modes. For the PFM mode, switching between the two beams shown in (**B**) from the beamsplitter rotates the plane of incidence of the beam with the surface by 180° and results in a reversal of contrast for regions of differing tilt directions in monolayers.

II. APPARATUS

A. Principles

A schematic of the entire apparatus is shown in Fig. 1. The assembly consists of a miniaturized Langmuir trough mounted on a vibrationally isolated table. For fluorescence operation, both unpolarized and polarized light sources are available for excitation. An optical microscope coupled to a low-light level camera is placed over the trough for imaging. For BAM operation a polarized laser beam is used for illumination, with a lens/camera system used for detection of the reflected light. Both cameras are coupled to a VCR/computer assembly for downloading images.

B. Film balance

The Langmuir trough is milled from a solid piece of Teflon of original dimensions 20 cm by 16 cm by 2 cm epoxied to a thin copper plate. The working surface area is 112 cm^2 with a subphase volume of approximately 150 ml. The well is tapered in the region used for imaging to both increase the compression ratio and to reduce surface convection. A Teflon barrier runs linearly along the top edge of the trough well. The barrier is spring loaded against the trough well and the ends of the barrier in contact with the well edges are beveled at an angle of approximately 10° to prevent leakage of surfactant from underneath. Movement of the barrier is accomplished by a model UT100 motorized translation stage purchased from Newport Klinger (Irvine, CA). The stage has a resolution of 0.1 μm, which translates to a resolution of approximately 1×10^{-3} $Å^2$/molecule for a typical experiment. The subphase temperature is read via thermistors located in the subphase. Temperature control of the subphase is achieved through the use of nine thermoelectric cooling (TEC) elements purchased from Marlow Industries (Dallas, TX). These elements are connected in series and located between a constant temperature water bath and the copper plate on which the trough is mounted. The trough can be operated in a temperature range of 10–50 °C. A piece of resistively heated glass purchased from Delta Technologies (Dallas, TX) is placed over the trough during experiments to eliminate condensation on the microscope objective; the coverglass is coupled to the moving barrier during experiments. The temperature of the glass is also read by a thermistor; it is typically maintained at a temperature slightly above the subphase temperature to reduce convective air currents above the monolayer. The surface pressure is measured by a Wil-

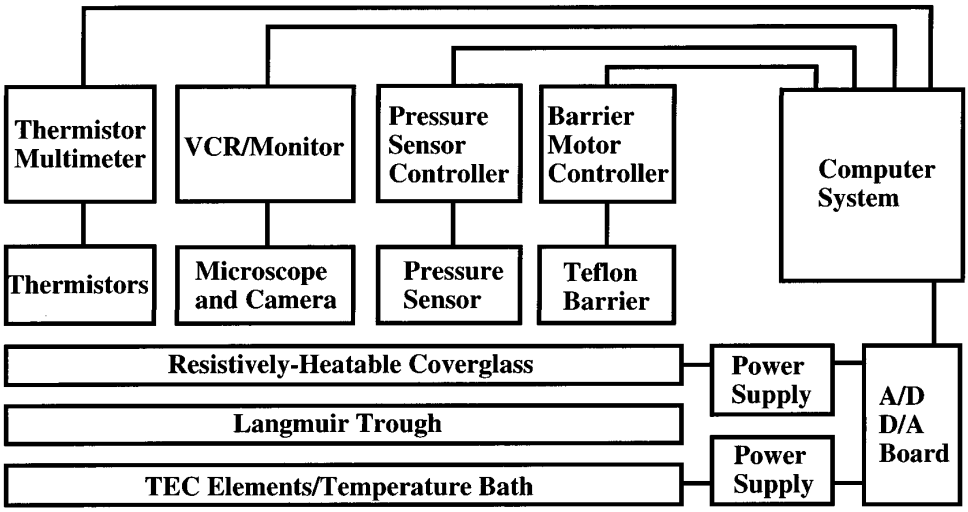

FIG. 2. A schematic of the computer interface system for the FM/PFM/BAM assembly.

helmy plate-type transducer purchased from R&K (Wiesbaden, Germany). The pressure sensor is mounted on the barrier to allow sampling of the monolayer through a hole in the coverglass.

C. Fluorescence and polarized fluorescence microscope operation

For both normal and polarized fluorescence operation, a Nikon Optiphot (Irvine, CA) optical microscope is positioned above the trough. A 40× power long working distance objective designed for use with fluorescence illumination is used. Focusing is done by mounting the trough on a motorized *xyz* translation stage purchased from Newport Klinger (Irvine, CA): the *z* axis is used for focusing, while the *x* and *y* axes are used for scanning over different regions in the monolayer. For normal fluorescence operation, a 100 W high-pressure mercury lamp is used for excitation. A dichroic mirror/barrier filter assembly is used to direct the excitation light onto the monolayer (with a normal angle of incidence) and to filter the emitted fluorescence. For polarized fluorescence operation, an Innova series 70 argon-ion laser from Coherent (Sunnyvale, CA) is used as the illumination source. A beam-splitter cube/mirror assembly is employed to allow for the plane of incidence of the beam to be rotated by 180° to allow for the detection of regions of different tilt directions in surfactant monolayers. In both cases, the emitted fluorescence is collected by the objective and detected via a low light level silicon intensified target (SIT) camera from Dage MTI (Michigan City, IN).

D. Brewster angle microscope operation

The argon-ion laser is also used as the light source for the BAM. A rotatable mirror and a polarizer purchased from Melles–Griot (Sunnyvale, CA) is placed between the laser and the trough to ensure that *p*-polarized light is incident on the monolayer at the Brewster angle (approximately 53° from vertical for a pure water subphase). Depending on the magnification required, either a simple lens (Melles–Griot) or a long focal length microscope objective (Nikon) is used to collect the weakly reflected light. An additional rotatable polarizer (Melles–Griot) positioned posterior to the objective is used as an analyzer to improve the contrast of the image. A Dage MTI (Michigan City, IN) model 72 charge-coupled-device (CCD) camera detects the image. This camera is mounted on a rotary stage to allow the CCD chip to be positioned parallel to the image plane of the monolayer to eliminate any longitudinal distortion effects. The BAM can be operated in conjunction with the normal fluorescence mode. Images for all three microscopy systems are recorded by a JVC super VHS VCR (Elmwood Park, NJ) and digitized via a Scion frame grabber (Frederick, MD). The resulting digitized images are processed and analyzed following a custom-designed protocol.

E. Computer interfacing

A block diagram of the interfacing scheme is displayed in Fig. 2. All parts of the combined assembly are under direct control of a single master operating program developed using the graphical programming system LABVIEW purchased from National Instruments (Austin, TX). Prior to beginning an experiment, the concentrations and molecular weights of the surfactants used are entered along with file saving information. During an experiment the main program loop displays the surface pressure, subphase and coverglass temperatures, barrier position, monolayer area, and other operating parameters in real time on a user-friendly front panel interface. The barrier speed and direction, the current sent to the TEC elements, and the voltage drop across the coverglass can be updated at any time. The surface pressure can be controlled to within ±0.5 mN/m via a proportional-integral-derivative (PID) algorithm that adjusts the barrier position to maintain a constant surface pressure. The subphase temperature can be controlled to within ±0.1 °C with a similar PID algorithm that adjusts the voltage sent to the TEC elements. An isotherm can be initiated and stopped at any time, the values of surface pressure and area are stored in an array and

TABLE I. Amino acid sequences of peptides derived from human SP-B and SP-C proteins (covalent fluorescent probe attachment sites are indicated by * above the specific peptide residue).

SP-B 1–25:

```
          *     *
F P I P L P Y C W L C R A L I K R I Q A M I P K G—COOH
1                                                  25
```

SP-B 1–78:

```
F P I P L P Y C W L C R A L I K R I Q A M I P K G A L R V
1
A V A Q V C R V V P L V A G G I C Q C L A E R Y S V I L L
30
D T L L G R M L P Q L V C R L V L R C S—COOH
59                                    78
```

SP-C:

```
      * *
F G I P C C P V H L K R L L A V A V A V A V A L A V A V A V G
1
A L L M G L—COOH
30       35
```

plotted upon termination of an experiment. Surface pressure or molecular area versus time data sets can also be recorded.

F. Synthesis and purification of surfactant peptides B and C

The amino-terminal segment of SP-B ($SP\text{-}B_{1-25}$) and SP-C were synthesized on a 0.25 mmol scale with an Applied Biosystems–Perkin-Elmer model 431A peptide synthesizer (Foster City, CA) using FASTMOC™ chemistry.[28] The synthetic $SP\text{-}B_{1-25}$ peptide, based on the 78 residue human sequence (Table I), was synthesized and purified using the procedure followed by Lipp *et al.*[24] A prederivatized Fmoc–Wang resin from Applied Biosystems–Perkin-Elmer (Foster City, CA) was used for synthesis. All amino acid residues were single coupled. After cleavage from the resin and high-performance liquid chromatography (HPLC) reverse phase single pass purification, the molecular mass of the reduced monomer was confirmed by FAB or electrospray mass spectrometry (UCLA Center for Molecular and Medical Sciences Mass Spectrometry) and the product was twice lyophilized from acetonitrile: 10 mmol HCL (1:1, v:v) to remove acetate counter ions. $SP\text{-}B_{1-25}$ was covalently labeled with maleimide-fluorescein probe obtained from Molecular Probes (Eugene, OR) as described previously.[24]

Synthetic SP-C peptide was based on the human sequence with a periodic substitution of alanine for valine (residues 15, 17, 19, 21, 23, 25, 27) in the hydrophobic polyvaline segment (Table I). A prederivatized Fmoc–Wang resin (Applied Biosystems–Perkin-Elmer) was used for synthesis of the peptide. Residues 1–28 of the hydrophobic polyvaline stretch were double coupled using the conventional FASTMOC™ cycles with the ABI 431A synthesizer while all other residues were single coupled.

After cleavage of the peptide from the resin, the crude material was purified by reverse-phase HPLC with a Vydac C4 column purchased from The Separations Group (Hesperia, CA) using a water-acetonitrile:isopropanol (1:1, v:v) gradient containing 0.1% trifluoroacetic acid. Palmitoylated SP-C was obtained by a modification of the protocol of Lapidot, Rapportort, and Wolman.[29] Synthetic SP-C peptide was reacted with twofold amounts of N-(palmitoyl) succinimide purchased from Sigma Chemical Co. (St. Louis, MC) in trifluoroethanol: 10 mM phosphate (9:1, v:v) buffer, *p*H 7, for 24 h. The molecular weight was determined by MALDI-TOF mass spectrometry.

The 4-chloro-7-nitrobenz-2-oxa-1,3-diazole (NBD chloride) adduct of SP-C was synthesized by reacting the reduced peptide with four fold NBD chloride (Molecular Probes) in dimethylformamide (peptide:probe, 1:4, mole:mole). The *p*H of the solution was adjusted to 7 with sodium hydroxide and stirred for 24 h at 35 °C. The resulting peptide derivative was then separated from unreacted NBD probe by gel filtration through a Sephadex G-10 column and the molecular mass confirmed by MALDI-TOF or FAB mass spectrometry.

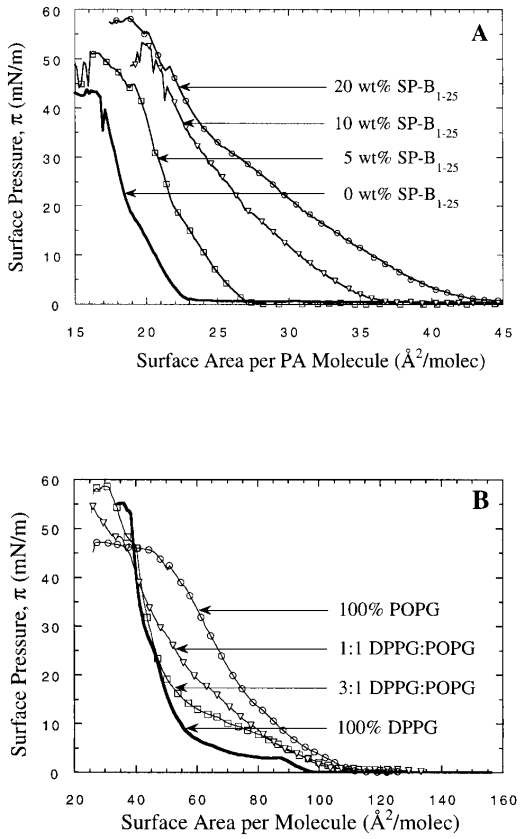

FIG. 3. Typical isotherms obtained from the FM/PFM/BAM assembly. (A) Surface pressure vs area per PA molecule isotherms at 16 °C on a buffered saline (0.15 M NaCl, *p*H=6.9) subphase as a function of $SP\text{-}B_{1-25}$ weight fraction for films containing: 0 (—), 5 (□), 10 (▽), and 20 (○) wt % $SP\text{-}B_{1-25}$. (B) Surface pressure vs area per molecule for mixed DPPG/POPG monolayers at 30 °C on a pure water subphase for films containing mole ratios of: 100% DPPG (—), 3:1 DPPG:POPG (□), 1:1 DPPG:POPG (▽), and 100% POPG (○).

III. OPERATION AND PERFORMANCE

A. Isotherms

Typical isotherms obtained from our system are shown in Fig. 3(A) for monolayers of palmitic acid (PA) on a buffered saline subphase (*p*H=6.9, 0.15 M NaCl) at 16 °C with

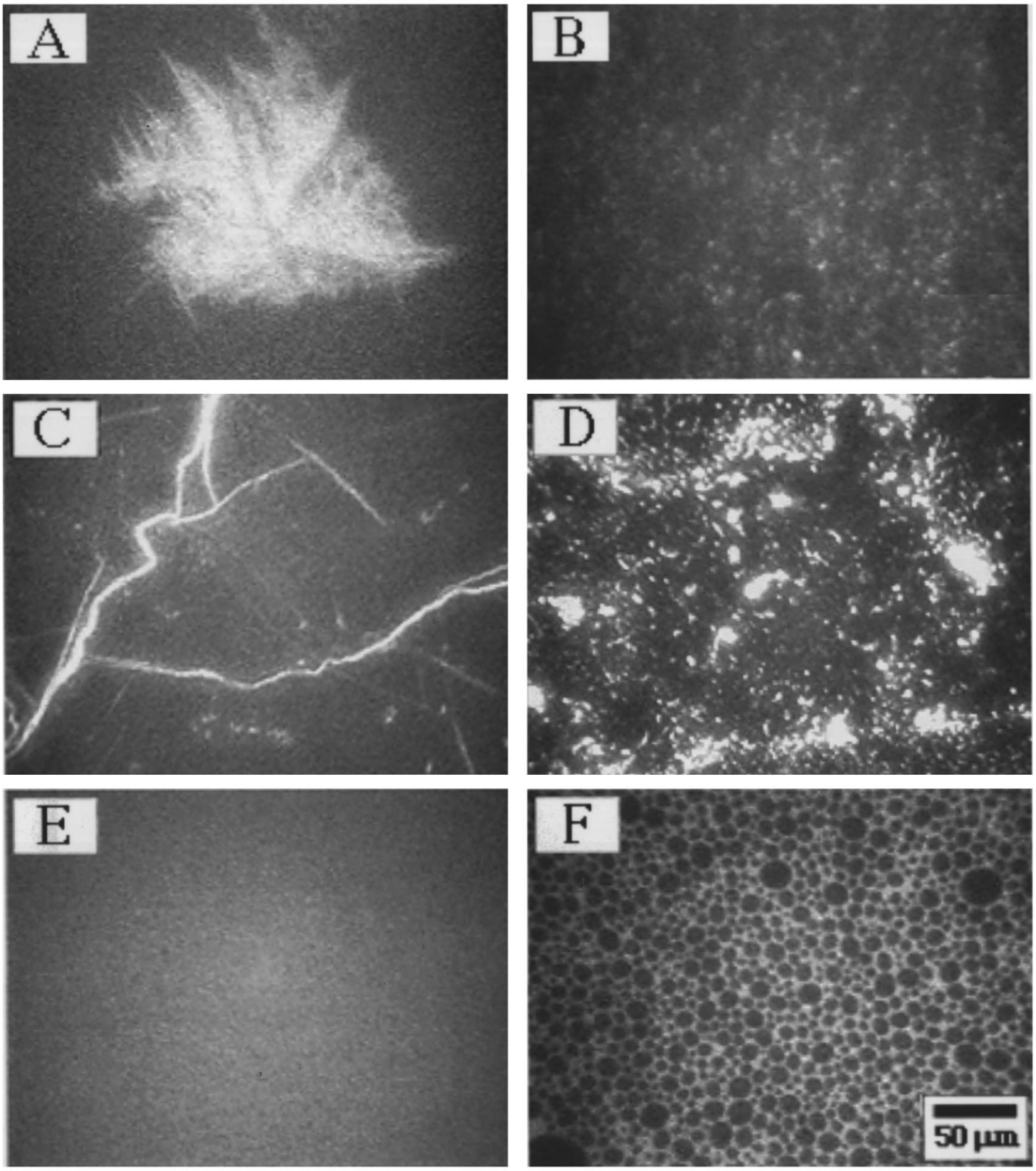

FIG. 4. Fluorescence images of the collapse behavior of PA and PA/SP-B_{1-25} monolayers. Images of the collapsed phase domains on a pure water subphase at 16 °C for (A) pure PA and (B) PA/20 wt % SP-B_{1-25}. Images from collapsed monolayers on a buffered saline (pH=6.9, 150 mM NaCl) subphase at 16 °C of (C) the fracture of a pure PA monolayer and (D) the nucleation and growth of collapsed domains for a PA/20 wt % SP-B_{1-25} film. Images taken at the lift-off point (point of initial surface pressure rise) for monolayers of (E) PA and (F) PA/20 wt % SP-B_{1-25} on a pure water subphase. All monolayers shown contain 0.5 mol % of the fluorescent probe NBD-hexadecylamine (NBD-HDA).

varying weight percentages (wt %) of SP-B_{1-25}, and Fig. 3(B) for mixed monolayers containing DPPG and 1-palmitoyl,2-oleoyl-phosphatidylglycerol (POPG) on a pure water subphase (18.2 MΩ resistivity Milli-Q water, Millipore Co., Medford, MA) at 30 °C. For the PA/SP-B_{1-25} system, isotherms indicate that the protein sequence has a drastic effect on the collapse behavior of these films, significantly increasing the collapse pressure on both pure water and buffered saline subphases [Fig. 3(A)]. The collapse pressures of a PA/20 wt % SP-B_{1-25} monolayer on buffered saline subphase are equivalent to that of DPPC at the same conditions, which effectively removes the driving force for squeeze-out of both PA and SP-B protein from LS monolayers.[30] For the DPPG/POPG system, the effect of the addition of increasing amounts of the unsaturated lipid POPG on the fluidity of monolayers of DPPG is clearly evident [Fig. 3(B)]. Additionally, the formation of plateau regions in the mixed DPPG/POPG monolayer isotherms at pressures near the collapse pressure of pure POPG can be seen; this plateau is traditionally given as evidence in support of the ''squeeze-out'' theory for the fluidizing components of LS.

B. Normal fluorescence microscopy images

The effect of the protein on the collapse behavior of PA monolayers is clearly evident via FM. As seen in Fig. 4, on

pure water subphases, PA monolayers collapse by a heterogeneous growth mechanism, with isolated domains nucleating and growing into large sizes. These domains appear to be crystalline via FM [Fig. 4(A)] and do not tend to reincorporate into the monolayer or respread. In the presence of 20 wt % SP-B_{1-25} protein, collapse occurs at much higher pressures, with collapsed domains nucleating homogeneously across the monolayer at high density [Fig. 4(B)]. These domains remain small upon compression past the point of collapse and tend to reincorporate more easily into the monolayer. Switching to a buffered saline subphase shifts the collapse mechanism of pure PA monolayers to a bulk folding and fracturing process [Fig. 4(C)]. Once again, the presence of protein raises the collapse pressure and alters the mechanism to a more uniform, homogeneous event [Fig. 4(D)] and facilitates reincorporation of the collapsed phase upon expansion.[24] The basis for the shift in the mechanism of the collapse process in the presence of protein is also shown by FM [Figs. 4(E) and 4(F)]. The protein creates a new fluid phase in PA/SP-B_{1-25} monolayers at low pressures on both pure water and buffered saline subphases, decreasing the size of and segregating the condensed domains prior to collapse. This segregation of the condensed phase domains prior to collapse reduces the likelihood of finding a heterogeneous nucleation site within a given domain, causing each domain to nucleate collapse homogeneously and independently.[24]

The FM system can also be used to determine the fate of selected components upon compression of mixed monolayers. A long-debated issue in LS research has been the fate of the unsaturated, fluidizing components upon compression of the LS monolayer. The squeeze-out hypothesis claims that the fluidizing components are somehow selectively removed from the LS monolayer to leave it enriched in DPPC which would facilitate the achievement of low surface tensions.[26] However, direct evidence for this process has been lacking; the occurrence of squeeze-out must usually be inferred from isotherm data. A recent Fourier transform infrared (FTIR) study of a mixed DPPC/POPG system has provided more direct evidence of this process; however squeeze-out must still be inferred to occur from the FTIR data.[27] Here we use our FM system to provide direct visual evidence that lipid squeeze-out occurs at least in binary mixtures of saturated and unsaturated PG. Images of monolayers containing DPPG and POPG at various ratios at a surface pressure of 40 mN m are shown in Fig. 5; this surface pressure corresponds to the point in the isotherm immediately prior to the formation of the squeeze-out plateau in mixed DPPG/POPG monolayers. As can be clearly seen in Fig. 5, the addition of POPG fluidizes the monolayers at this pressure; a pure DPPG monolayer exists entirely in a condensed state at this pressure while a 1:1 mixture of DPPG:POPG is approximately 50% condensed and 50% fluid.

Figure 6 reveals the fate of this fluid phase upon progression through the squeeze-out plateau for the case of a 3:1 DPPG:POPG film. At the beginning of the plateau, regions of the fluid phase in the interstitial regions can be seen to form three-dimensional phases that flow underneath the monolayer; the focal plane of these structures is immediately below the monolayer [Fig. 6(A)]. Upon further compression,

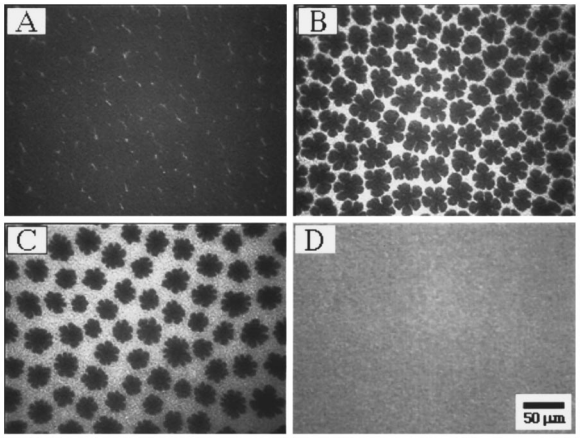

FIG. 5. Fluorescence images of mixed DPPG/POPG monolayer systems. Images taken at 30 °C on pure water subphases at a surface pressure of 40 mN/m of monolayers of mole ratios: (A) 100% DPPG, (B) 3:1 DPPG:POPG, (C) 1:1 DPPG:POPG, and (D) 100% POPG. All monolayers contain 0.5 mol % of the fluorescent probe NBD-PG.

more of the fluid phase is removed into the subphase, forming long, wormlike regions that flow underneath the condensed phase domains but still seem to be attached to the monolayer [Fig. 6(B)]. Once the plateau region is left, the condensed domains are now close packed, and the wormlike phase begins to detach from the monolayer and flow along with the subphase; they can be seen to undergo Brownian motion and there are now several focal planes of these objects extending into the subphase [Fig. 6(C)]. The eventual collapse of the monolayer seems to greatly accelerate this process; large areas of the monolayer can be seen to detach and enter the subphase, with wormlike shapes being seen several microns below the surface [Fig. 6(D)]. This process seems to be irreversible; once the squeezed-out and collapsed

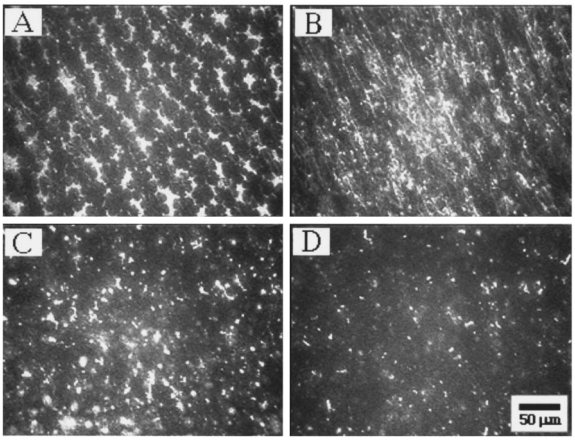

FIG. 6. A progression of fluorescence images of the squeeze-out of POPG from a 3:1 DPPG:POPG monolayer containing 0.5 mol % NBD-PG at 30 °C on a pure water subphase. (A) An image taken at the beginning of the squeeze-out plateau shown in the corresponding isotherm from Fig. 4(B), showing the formation of wormlike three-dimensional bulk phases below the monolayer. (B) An image taken at the end of the plateau region showing squeeze-out of the majority of the bright phase from the interstitial regions between the condensed phase domains. (C) An image showing the detached wormlike structures flowing in the subphase below the monolayer before collapse. (D) An image taken after collapse of the monolayer showing the presence of lipid structures well below the monolayer.

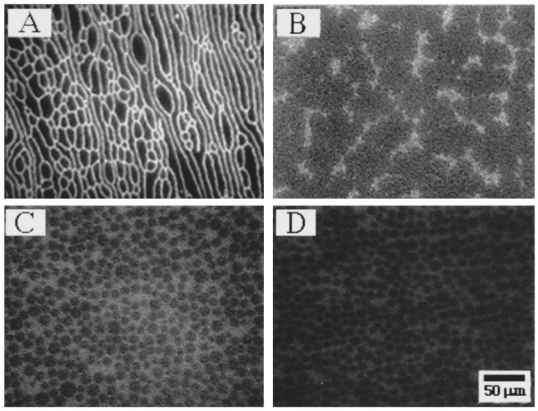

FIG. 7. Fluorescence images of monolayers containing fluorescently labeled LS proteins SP-B_{1-25} and SP-C. (A) An image of a fluorescein-SP-B_{1-25} (F-SP-B_{1-25}) monolayer on a pure water subphase at 23 °C showing the formation of a ''stripe'' phase at low surface pressures. (B) An image of a monolayer of DPPG/10 wt % NBD-SP-C taken immediately prior to collapse (π=60 mN/m) on a pure water subphase at 37 °C. Images of a monolayer of PA/20 wt % F-SP-B_{1-25} also containing 0.5 mol % Texas-red DPPE on a pure water subphase at 28 °C showing the fluorescence from (C) the lipid probe and (D) the fluorescently labeled protein.

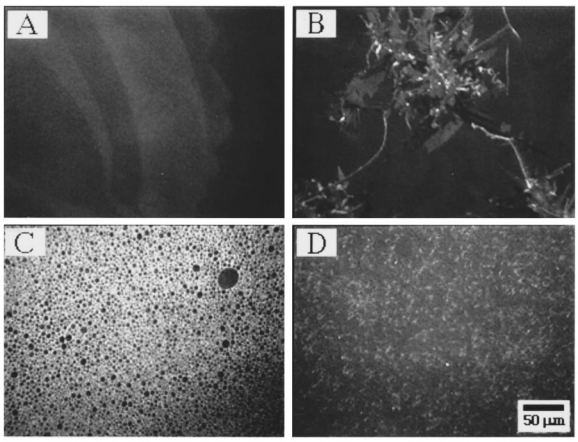

FIG. 8. Polarized fluorescence images of the collapse behavior of PA and PA/SP-B_{1-25} monolayers. Images of a PA film on a pure water subphase at 16 °C (A) at a pressure of 15 mN/m in the liquid-condensed phase (with contrast resulting from domains of differing tilt direction), and (B) after collapse of the monolayer, showing the growth of a tilted collapsed phase domain. Images of a PA/20 wt % SP-B_{1-25} film on a pure water subphase at 16 °C (C) at a pressure of 15 mN/m (showing a lack of tilt contrast within the small condensed domains), and (D) after collapse of the monolayer, showing the homogeneous distribution of small collapsed phase domains.

phases detach from the monolayer they form very stable aggregates in the subphase that do not tend to reincorporate into the monolayer upon reexpansion. However, although squeeze-out occurs for this binary lipid system, our results for PA/SP-B_{1-25} monolayers clearly demonstrate the fact that LS proteins can have drastic effects on the phase behavior of the fluidizing lipids of LS. Current work in our laboratory is centered on determining if LS proteins SP-B and SP-C may interact with unsaturated lipids such as POPG in a similar fashion to prevent their squeeze-out from the LS monolayer.

C. Fluorescent labeling of LS proteins

Our ability to label synthetic versions of LS proteins SP-B and -C at specific residues allows us to unequivocally determine the location and phase preferences of these components in mixed lipid/protein monolayers. Monolayers of these labeled proteins alone can display coexisting phases. Fluorescein-labeled SP-B_{1-25} (F-SP-B_{1-25}) forms stripe phases of a constant width [Fig. 7(A)]; this indicates a delicate balance between line tension and electrostatic repulsion within the domains. The addition of NBD-labeled SP-C (NBD-SP-C) to DPPG monolayers allows us to determine the phase partitioning preference of the protein and ascertain whether this component is squeezed-out of saturated lipid monolayers. NBD-SP-C partitions into the expanded phase during the liquid-expanded (LE)/liquid-condensed (LC) phase transition of DPPG and creates a bright fluid phase that persists to high pressures and segregates the condensed phase domains right up to collapse of the monolayer. An image taken past the squeeze-out plateau region for a DPPG/10 wt % NBD-SP-C monolayer on a physiological subphase (buffered saline, 37 °C) shows the persistence of this phase right up to collapse of the monolayer [Fig. 7(B)], and does not exhibit the squeeze-out behavior (formation of bright regions below the monolayer) seen in the mixed POPG/DPPG system (see Fig. 6).

Dual probe experiments, in which monolayers contain a fluorescent lipid probe and fluorescently labeled protein, allow for an unambiguous identification of the partitioning preference of the protein with respect to the lipid phases. The rapid switching of the appropriate fluorescence filter cube assemblies allows for the simultaneous observation of the lipid and the protein fluorescence from the monolayer. Images of a monolayer of PA/F-SP-B_{1-25} containing 0.5 mol % Texas-red dipalmitoylphosphatidylethanolamine (DPPE) show that the protein partitions into the disordered fluid phase under all experimental conditions [Figs. 7(C) and 7(D)]. As previously discussed, this protein-rich phase persists to high pressures, effectively partitioning and separating the solid phase domains immediately prior to collapse.

D. Polarized fluorescence microscopy images

For condensed lipid phases in which the molecules are tilted in a specific direction with respect to the surface normal, the use of polarized light as the fluorescence excitation source leads to a contrast between regions of different tilt directions. For the LS system, both monolayers of DPPC and PA form tilted condensed phases that can be viewed with PFM. For PA, PFM allows us to determine the influence of lipid molecule tilt on both the nature of the nucleation of collapse and the lack of reincorporation of the collapsed phase on reexpansion. For pure PA monolayers at low temperatures, the LC phase consists of domains of differing tilt directions bordering at defect lines and points [Fig. 8(A)]. Upon transition to the untilted solid phase prior to monolayer collapse, if these defect points are not allowed to anneal out, they may act as heterogeneous nucleation sites and allow collapse to occur at lower pressures. Additionally, PFM reveals that the collapsed phase itself is tilted, while the underlying monolayer is untilted [Fig. 8(B)]. This means that the collapsed phase is at a lower packing density with respect to

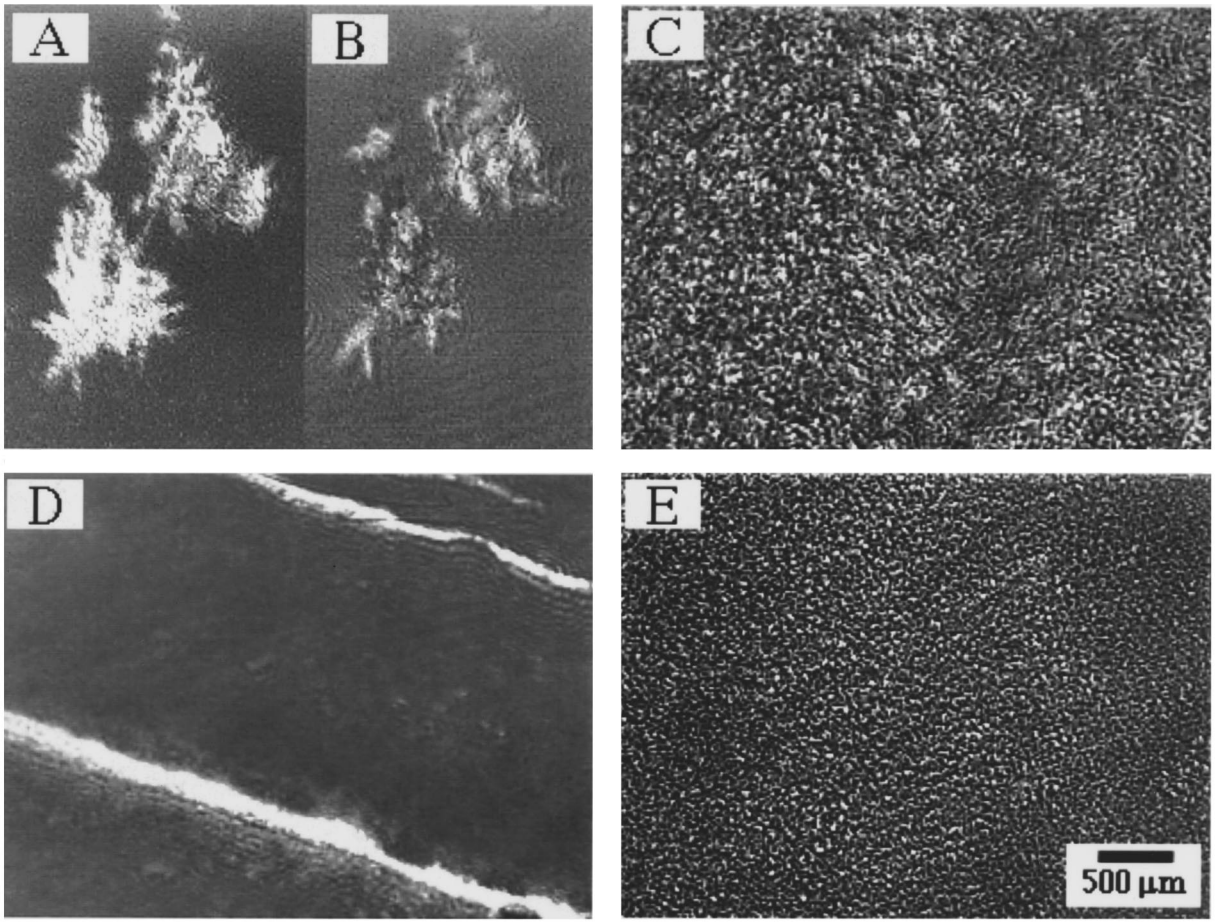

FIG. 9. Brewster angle microscope images of the collapse behavior of PA and PA/SP-B_{1-25} monolayers. Images of a collapsed phase domain from a PA film on a pure water subphase at 16 °C, with the analyzer rotated between images (A) and (B) to show the tilt contrast of the domain. (C) Image of a PA/20 wt % SP-B_{1-25} film on a pure water subphase at 16 °C showing the growth of the uniform collapsed phase. Images from monolayers on buffered saline subphases at 16 °C showing (D) bulk fracture of a PA monolayer and (E) nucleation and growth of a collapsed phase for a PA/20 wt % SP-B_{1-25} film.

the monolayer, and would have to contract in order to be reincorporated into the monolayer upon expansion. In the presence of protein, the condensed phases are individually either untilted or of uniform tilt [Fig. 8(C)]. This removes the influence of any tilt defects on the collapse nucleation process and requires each domain to nucleate collapse homogeneously. Additionally, the collapsed phase domains themselves do not appear to be tilted [Fig. 8(D)], which in combination with their smaller size may ease their reincorporation into the monolayer.

E. Brewster angle microscopy images

A significant concern with the use of FM and PFM for the study of surfactant monolayers has been the possibility of artifacts due to the addition of foreign probe molecules to the system. BAM provides equivalent information to PFM without requiring the addition of a foreign probe molecule. However, due to the fact that the light path is at the Brewster angle with respect to the object plane, the entire image is not in focus at the same time; this effect worsens as the depth of focus decreases at higher magnifications. Thus, it is difficult to achieve images with as high a magnification and resolution as with FM or PFM. Despite this, BAM can be used to confirm that the probe molecules, present at low concentrations, do not have an influence on the morphologies observed in lipid and protein films via FM and PFM, and to provide images at larger length scales. In all cases so far in our laboratory, BAM has provided completely analogous images of monolayers of various components of LS to those obtained with FM and PFM. This confirmation is of particular importance for the study of collapse of PA/SP-B_{1-25} films; sites of accumulation of fluorescently labeled molecules could potentially act as heterogeneous nucleation sites. However, at all experimental conditions BAM images of collapse show a similar shift in collapse mechanism as seen with FM and PFM. On pure water subphases, BAM images show the growth of large, isolated, tilted collapsed phase domains for pure PA films [Figs. 9(A) and 9(B)]. On buffered saline subphases, BAM images further reveal the macroscopic dimensions of the fracture cracks in collapsed films of pure PA [Fig. 9(D)]. For both subphases, in the presence of SP-B_{1-25}, BAM images show the homogeneous and uniform nature of the growth of the collapsed phase domains at a much higher nucleation density [Figs. 9(C) and 9(E)].

IV. DISCUSSION

We have shown that our combined FM, PFM, and BAM/Langmuir trough assembly is an ideal system for the study of

LS monolayers. The phase behavior of mixed lipid and protein monolayers can be studied under a range of conditions, including physiological (37 °C, buffered saline subphase). The complementary information provided by FM, PFM, and BAM can be used to identify the composition of certain phases and to determine the orientation of condensed phases. Our ability to specifically label LS proteins with fluorophores, and to conduct dual-probe experiments with this system, further facilitates the identification of the composition of coexisting phases and the phase partitioning characteristics of the proteins with respect to the lipid phases. This combined approach allows us to determine the mechanism by which model LS monolayers function, and to answer physiologically relevant questions such as the fates of the fluidizing components of LS at high monolayer pressures (whether they are squeezed-out or act synergistically with LS proteins to achieve higher monolayer pressures). This integrated assembly will allow us to systematically study multicomponent model LS monolayers and relate the observed morphologies and phase behavior to the presence of specific components.

ACKNOWLEDGMENTS

The authors would like to thank D. K. Schwartz and C. M. Knobler for access to their PFM and BAM systems and for their helpful discussions. The Langmuir trough was constructed here at UCSB by A. S. Weinberg and H. R. Stuber in the physics mechanical shop. M.M.L. was supported by a University of California Regents Fellowship and a Corning Foundation Fellowship. K.Y.C.L. was supported by a University of California Presidents Postdoctoral Fellowship. A.J.W. was supported by NIH HL 55534 and the peptide synthesizer was acquired by a NIH small equipment grant GM 50483. J.A.Z. was supported by NIH HL 51177.

[1] J. Swalen *et al.*, Langmuir **3**, 932 (1987).
[2] H. Möhwald, Annu. Rev. Phys. Chem. **41**, 441 (1990).
[3] H. M. McConnell, Annu. Rev. Phys. Chem. **42**, 171 (1991).
[4] S. Hénon and J. Meunier, Rev. Sci. Instrum. **62**, 936 (1991).
[5] D. Hönig and D. Möbius, J. Phys. Chem. **95**, 4590 (1991).
[6] D. Möbius and H. Möhwald, Adv. Mater. **3**, 19 (1991).
[7] R. W. Weis, Chem. Phys. Lipids **57**, 227 (1991).
[8] C. M. Knobler and R. Desai, Annu. Rev. Phys. Chem. **43**, 207 (1992).
[9] H. Möhwald, Rep. Prog. Phys. **56**, 653 (1993).
[10] D. W. Grainger, A. Reichert, H. Ringsdorf, and C. Salesse, Biochim. Biophys. Acta **1023**, 365 (1990).
[11] A. Reichert, H. Ringsdorf, and A. Wagenknecht, Biochim. Biophys. Acta **1106**, 178 (1992).
[12] S. Riviere, S. Hénon, J. Meunier, D. K. Schwartz, M. W. Tsao, and C. M. Knobler, J. Phys. Chem. **101**, 10045 (1994).
[13] D. K. Schwartz, M. W. Tsao, and C. M. Knobler, J. Phys. Chem. **101**, 8258 (1994).
[14] K. Nag, C. Borland, N. Rich, and K. M. Keough, Biochim. Biophys. Acta **1068**, 157 (1991).
[15] J. Perez-Gil, K. Nag, S. Taneva, and K. M. Keough, Biophys. J. **63**, 197 (1992).
[16] K. Nag and K. M. Keough, Biophys. J. **65**, 1019 (1993).
[17] D. L. Shapiro, in *Surfactant Replacement Therapy*, edited by D. L. Shapiro and R. H. Notter (Liss, New York, 1989), p. 1.
[18] S. Hawgood and K. Shiffer, Annu. Rev. Physiol. **53**, 375 (1991).
[19] T. E. Weaver and J. A. Whitsett, Biochem. J. **273**, 249 (1991).
[20] A. J. Waring, W. Taeusch, R. Bruni, J. Amirkhanian, B. Fan, R. Stevens, and J. Young, Peptide Res. **2**, 308 (1989).
[21] A. Takahashi, A. J. Waring, J. Amirkhanian, B. Fan, and H. Taeusch, Biochim. Biophys. Acta **1044**, 43 (1990).
[22] A. J. Waring, L. M. Gordon, H. W. Taeusch, and R. Bruni, in *The Amphipathic Helix*, edited by R. Epand (Chemical Rubber, Boca Raton, FL, 1993), p. 143.
[23] L. M. Gordon, S. Horvath, M. Longo, J. A. Zasadzinski, H. W. Taeusch, K. Faull, C. Leung, and A. J. Waring, Protein Sci. **5**, 1662 (1996).
[24] M. M. Lipp, K. Y. C. Lee, J. A. Zasadzinski, and A. J. Waring, Science **273**, 1196 (1996).
[25] L. M. van Golde, J. J. Batenburg, and B. Robertson, Physiol. Rev. **68**, 374 (1988).
[26] J. Egberts, H. Sloot, and A. Mazure, Biochim. Biophys. Acta **1002**, 109 (1989).
[27] B. Pastrana-Rios, C. R. Flach, J. W. Brauner, A. J. Mautone, and R. Mendelsohn, Biochemistry **33**, 5121 (1994).
[28] C. G. Fields, D. H. Lloyd, R. L. MacDonald, K. M. Ottenson, and R. L. Noble, Peptide Res. **4**, 95 (1991).
[29] Y. Lapidot, S. Rapportort, and Y. Wolman, J. Lipid Res. **8**, 142 (1967).
[30] M. L. Longo, A. M. Bisagno, J. A. Zasadzinski, R. Bruni, and A. J. Waring, Science **261**, 453 (1993).